PHYSICAL REVIEW E **86**, 065401(R) (2012)

Pearl-necklace-like structures of microparticle strings observed in a dc complex plasma

M. A. Fink, S. K. Zhdanov, M. H. Thoma,* H. Höfner, and G. E. Morfill
Max Planck Institute for Extraterrestrial Physics, 85741 Garching, Germany
(Received 12 October 2012; published 19 December 2012)

The observation of a well-developed treelike string structure supported by a gas flow in a three-dimensional dc complex plasma is presented. The dynamically stable strings, comprising 10–20 particles, were up to 5 mm long. The experiments were performed using neon gas at a pressure of 100 Pa and melamine-formaldehyde particles with a diameter of 3.43 μm. Inside the discharge glass tube a nozzle had been built in to supply the controllable gas (plasma) flux intensity distribution along the tube. The walls of the nozzle were transparent for the laser light illuminating the particles. That gave the opportunity to closely study the particle dynamics deep inside the nozzle.

DOI: 10.1103/PhysRevE.86.065401 PACS number(s): 52.27.Lw, 52.27.Gr, 36.40.Mr

I. INTRODUCTION

A complex (dusty) plasma is a weakly ionized gas, incorporating solid particles [1,2]. In experimental investigations of complex plasma dynamics and self-organization the particle size is usually of a micron to some tens of microns. In dc and rf complex plasmas used for those studies the particles are negatively charged, hence they have to be externally confined. The external confinement forces deeply affect the global configuration of the complex plasma on a large scale [3]. The internal structure, in turn, is mostly determined by the mutual particle-particle interactions consisting of isotropic (repulsive) and anisotropic (attractive, wake-mediated) forces, as recent detailed studies demonstrated [4–9]. This delicate interplay of isotropic and anisotropic forces gives rise to different competing symmetries, patterns, and phase transitions [10–16]. Dynamically driven clusters with a well-developed string structure have been recently studied in an rf complex plasma [17]. Self-organization through the formation of dust striations in the form of chains have been observed for the first time in sparks [18].

Structuring through the formation of strings, filaments, and patterns (lattices) formed by the interacting strings is one of the basic processes in many systems as diverse as electrons on superfluid helium [19], current-carrying plasmas [20,21], superconductors [22], laser pulse filamentation in various transparent media [23], colloids [24], and temporal networks [25]. The large-scale Universe structuring (with galaxies and galaxy clusters as structuring elements) through cold-dark-matter filament formation (dark-matter skeleton) has also been discovered recently [26].

Commonly, the neutral gas in complex plasma dynamical studies is considered as a passive factor, resulting mainly in the frictional reduction of the microparticles' kinetic energy. Only recently active applications of the gas component of the complex plasma have been started to control and manipulate the particles. Among those are active experiments intended to investigate the particle cloud convection in response to gas creep [27,28], the cloud rotation as a whole in response to the neutral gas drag [8], or even to mimic the magnetization of the heavy dust particles in a complex plasma, making use of the frictional coupling between a complex plasma and the neutral gas [29].

In this Rapid Communication we report on the structuring of a dc complex plasma using particle clusters dynamically equilibrated by the neon gas flux at pressures of 80–100 Pa. The experiments were conducted using a laboratory version of the PK-4 design [27,30,31]. The elongated form of the PK-4 discharge tube (with an aspect ratio as large as 3 : 35) provides a unique experimental design for studying the propagation of different kinds of dust waves and flow effects. In particular, there is an opportunity to build-in a nozzle, effectively redistributing the gas flow along the discharge axis. It can be used to create and control a force which is powerful enough to counteract, e.g., gravity or the forces of the electric fields of the discharge—the main unavoidable driving forces in the ground-based experiments with dc complex plasmas. Using small particle clusters as a probe of the axial discharge field distribution is also another opportunity that is briefly discussed here.

II. EXPERIMENTAL CONDITIONS

The experiments were performed using the Plasmakristall 4 (PK-4) experimental device that exploits the positive column of a high-voltage dc discharge to produce complex (dusty) plasmas. A photograph of the experiment geometry is shown in Fig. 1. In the heart of the setup is the glass discharge tube. The glass tube provides very good access for optical diagnostics. The main part of the tube designed for experiments has a length of 35 cm and an inner diameter of 3 cm. It is terminated by two glass knees (the lower one of them is seen in Fig. 1). The disk-shaped discharge electrodes are mounted at the ends of the tube at a total distance of 732 ± 4 mm between them (along the discharge path); the lower one is used as the anode. Two optical ports offer access for laser illumination and manipulation, and four particle dispensers allow the use of different microparticles. A gas supply system with an adjustable gas flow ensures the purity of the gas (neon) and offers an additional way of introducing controllable gas flow to the discharge (the gas inflow is in the lower part of the tube). As an example of the gas flow controller characteristic, see Fig. 2. Two CCD cameras record the microparticles.

The dc discharge is operated with a regulated current of $I_{dc} = 1.1$ mA, corresponding to a voltage of about $U_{dc} \cong 1500$ V. The plasma parameters, i.e., electron temperature and density and the longitudinal electric field in the positive column of the dc discharge without the nozzle,

*thoma@mpe.mpg.de

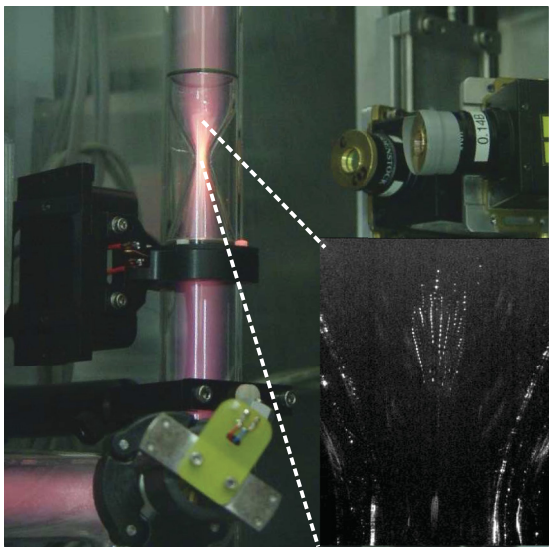

FIG. 1. (Color online) The heart of the PK-4 laboratory setup. The straight part of the glass discharge tube with a diameter of 30 mm and a length of 350 mm is oriented vertically. The glass nozzle implemented inside the tube (by means of two Viton rings, on the top and bottom of the nozzle) has a diameter of 5 mm in the nozzle throat. Inset: A snapshot of the particle positions located slightly above the nozzle throat. The field of view is 12.67×9.50 mm^2. The particles form a cluster which is seen in the inset close to the center line as a treelike system of bright spots arranged as a pearl necklace. The glass nozzle is overall transparent and seen therefore only as (parabolalike) sets of bright reflections to the left and to the right from the cluster.

have been determined by Langmuir probe measurements in ground-based laboratory experiments in the absence of particles by Usachev *et al.* [30]. Using the results of these measurements one can estimate that far away from the nozzle the longitudinal electric field is given by $E \simeq 2.1$ V/cm.

A. Complex plasma parameters

A controlled gas pressure was chosen at a level of 100 Pa and a flow rate of 0.14 sccm. Monodisperse melamine-formaldehyde particles with a diameter of 3.43 μm ($\pm 2\%$) and a mass of $m = 3.2 \times 10^{-11}$ g were injected into the dc discharge plasma in the vicinity of the cathode above the nozzle. After the injection the particles rapidly fell down in the direction of the anode driven by the dc electric field of the discharge and by gravity. Then they were stopped and partly trapped deep inside the nozzle at a distance of ~24–29 mm

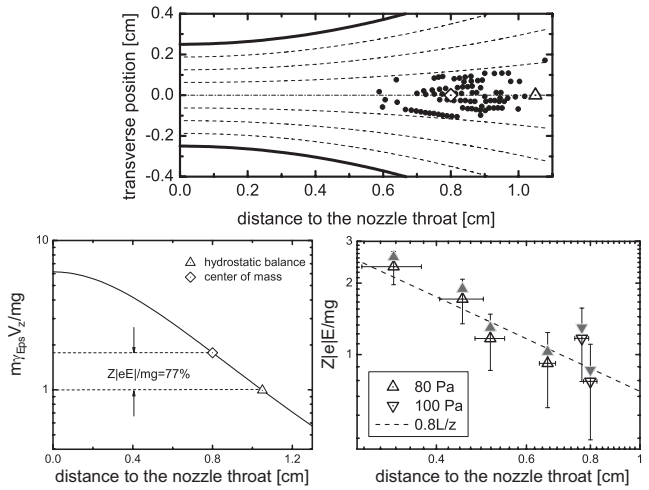

FIG. 3. Upper: The nozzle boundary (bold lines) and the gas flow lines (dashed) inside the nozzle superimposed with the traced particle positions (black dots). Lower left: Sketch of the electric force diagnostics. The solid line shows the profile of the normalized gas drag force. The "hydrostatic balance" point $mg = m\gamma V_z$ is indicated by the open triangle ($mg \simeq 310$ fN). The revised force balance $mg + Z|eE| = m\gamma V_z$ at the actual position of the cloud center of mass (the open diamond) allows one to estimate the magnitude of the electric forces. Lower right: The normalized electric force distribution along the nozzle axis (the open triangles). The same, corrected for the ion drag force estimated by using Refs. [37,38] (the gray triangles). The dashed line $E \sim z^{-1}$ is shown to guide the eye.

below the nozzle entrance by the steadily amplifying gas flow. The gas damping rate is estimated to be $\gamma_{Eps} \simeq 227$ s^{-1} [32]. The large value of the gas drag coefficient leads to a strong frictional coupling of the particles to the gas.

The particle cloud was illuminated by a laser sheet (wavelength: 686 nm; output power: 20 mW) with a width of 100 μm [full width at half maximum (FWHM)] and recorded by a CCD camera at a frame rate of 120 fps and a spatial resolution of the video recording system of 19.8 μm/px (39.6 μm/px) along (transverse to) the nozzle axis. On average over 50–100 particles (see Fig. 3) were tracked in each frame and traced from one frame to another to calculate the particle velocity. During the experiments the injected particles formed a long-living cone-shaped cluster with a major length of 3.5–5 mm, with the cone apex oriented along the nozzle axis and pointed to towards the nozzle throat; the cone opening angle is $\theta \approx 30^\circ$.

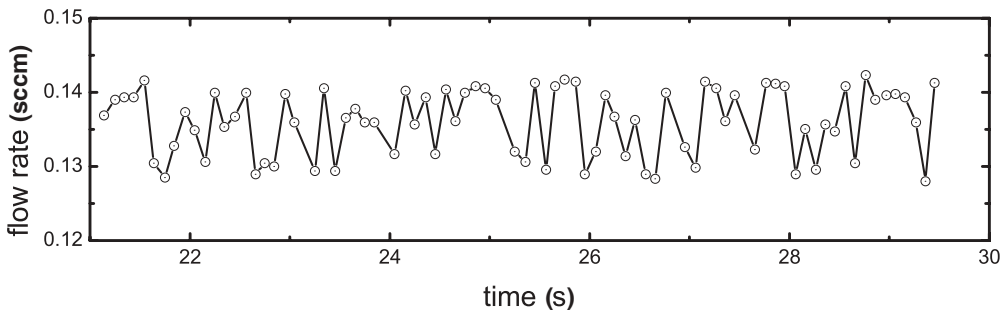

FIG. 2. An example of the gas flow controller (MKS1178BX) characteristics. The oscillation's "quasi"-period is 0.4 ± 0.04 s.

The cloud was highly inhomogeneous, consisting of a system of clearly visible separated strings. The in-string particle separation Δ slightly varied during the observation time; on average, $\Delta = 160$–200 μm. Using Refs. [30,31] the electron density n_e and the electron temperature T_e were estimated as $n_e = (3$–$4) \times 10^8$ cm^{-3} and $T_e = 6$ eV. Following Refs. [33,34] and using the parameters listed above, we estimated the particle charge to be in the range of $Ze = (3000$–$4000)e$, where e is the elementary charge.

B. Nozzle geometry

The nozzle, as any other kind of discharge tube constriction, either in the form of an orifice [35] or a sharp change in the diameter of the tube [36], can cause a strong influence on the discharge conditions locally. This is immediately evident from the enhanced radiation from the vicinity of the nozzle (see Fig. 1). The most probable explanation is that the constriction results in the development of an electron-accelerating potential drop, as it has been suggested in Ref. [35].

The built-in nozzle in our conditions has the following dimensions: The throat diameter is 5 mm, the total exit (entrance) diameter is 30 mm, the wall thickness is $\simeq$2 mm, and the nozzle total length is 70 mm. The particles are stably confined inside the diverging section of the nozzle (see Fig. 1). At the position of the particle cloud the nozzle profile is approximately parabolic with the internal radius introduced by the relationship

$$R_{\text{nozzle}} = R(z) \simeq R_0 \left(1 + \frac{z^2}{L^2}\right), \tag{1}$$

where $R_0 = 2.5$ mm, $L = 8.6$ mm, and $z = 0$ is chosen to be at the nozzle throat. Note that relationship (1) is applicable only at distances $z < L$ from the nozzle throat. After the transition region located at $L < z < 2L$, the nozzle wall profile converges further to the discharge tube wall radius at $z = 35$ mm. In the following we only use distances $z < L$. The gas flow through the nozzle in our conditions can be considered approximately as incompressible viscous (see, e.g., Ref. [39]). Since $\max(|dR/dz|) < 1$, one can use the simplified theory of the nozzle with a slowly varying profile. The gas velocity components inside the nozzle can be approximated then as

$$V_z = \frac{\partial(r\chi)}{r\partial r}, \quad V_r = -\frac{\partial\chi}{\partial z},$$
$$\chi = \frac{1}{2} V_j \frac{D^2}{R^2(z)} r \left(1 - \frac{1}{2}\frac{r^2}{R^2(z)}\right), \tag{2}$$

where χ is the flux function, r, z are the (cylindrical) coordinates, D is the discharge tube diameter, and $V_j = \frac{4j}{\pi D^2 n}$ is the equivalent flow velocity, which corresponds to the supplied gas flux j at a given gas density n. The flow lines computed according to (2) are shown in Fig. 3.

III. CLOUD POSITION AND STABILITY

A. Axial force balance

The cloud shown in Fig. 1 (inset) as a whole appeared to be surprisingly stable. Its center of mass is positioned on the nozzle symmetry line at $\langle z \rangle = 8.0 \pm 0.2$ mm away from the nozzle throat. According to (2) this corresponds to the gas axial velocity of the order of $V_z \simeq 7.7$ cm/s. Note that the electric field force is an essential component of this balance: Purely "hydrostatic" balance, $m\gamma_{\text{Eps}} V_z = mg$, is not enough to explain the actual position of the cluster center of mass (see Fig. 3).

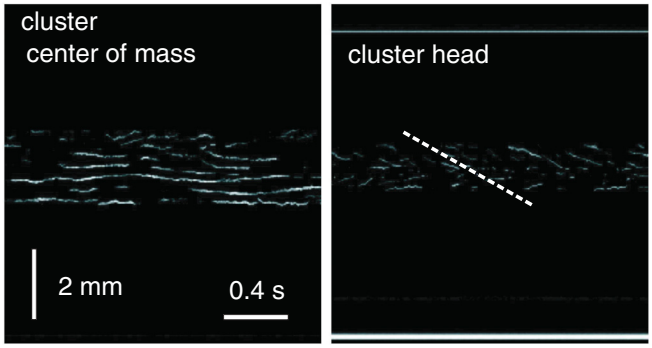

FIG. 4. (Color online) Time-space plots obtained at the central part of the cluster (left) and at the cluster head (right). The weak instability of the vertical cloud position, as well as the weak flatter of the particle chains, is due to imperfectness of the gas flow controller. A near-axis particle local systematic drift is also noticeable, approximately, on average, at 2–3 mm/s. The dashed line is shown to guide the eye corresponds to $V_D = 2.5$ mm/s. The time is running from left to right in both panels.

The position of the cluster center of mass along the nozzle axis ($r = 0$) has to be described by the extended balance (reduced to one particle) including electric field forces:

$$F_z \equiv m\gamma_{\text{Eps}} V_z - mg - Z|e|E_z = 0, \tag{3}$$

with the vertical projections of the electric field force ZeE_z [40], gravity, and the counteracting gas drag $m\gamma_{\text{Eps}} V_z$. Here V_z is the vertical projection of the gas velocity taken at the nozzle axis, defined by Eq. (2). Since the actual position of the cluster center of mass can be obtained from observations, relationship (3) can be used to estimate the electric field strength at the cluster center of mass. It can be used as an effective tool for diagnostic purposes as it is illustrated in Fig. 3: Measured vertical positions of the center of mass of several particle clusters subjected to different gas fluxes allow us to extract the distribution of the electric field along the nozzle axis. The experiments were performed for the range of Ne gas fluxes from 0.09 to 1.6 sccm at 80–100 Pa.

The stability of the vertical balance also is not difficult to address. Upstream from the nozzle throat, the gravity is dominating; downstream both the electric field force and the gas drag are stronger. Hence, the balance is stable when the downstream variation of the gas head is larger: $m\gamma_{\text{Eps}}\delta(V_z) > \delta(Z|e|E_z)$. It is easy to control, e.g., by adjusting the gas flow.

The weak vertical oscillations of the cloud center of mass is easy to trace, for example, by using the time-space plots shown in Fig. 4. The plots were assembled by adding up the measured pixel intensities for every recorded frame from a narrow slab of 12 px width taken transverse to the nozzle axis [41] at the positions indicated in Fig. 4. The period of the global oscillations appeared to be of the order of 0.4 s. Hence, it can be well explained by imperfectness of the gas flux controller.

It is worth noting that in general the electric field of the dc discharge is the sum of the resistive component and

the ambipolar diffusion component [35]. Inside the nozzle the plasma becomes highly inhomogeneous, enhancing the magnitude of the ambipolar field.

B. Transverse stabilization

The observation showed that transversally the cluster is also stable. An additional stabilizing factor, compensating the transverse instability of the "hydrostatic" balance, comes from the transverse repulsive confinement that appears due to negative charging of the walls of the nozzle. The deeper into the nozzle, the stronger is the transverse electric field. It explains approximately the conic form of the particle cluster at the height of its center of mass (Fig. 3) by the cylindrical radius $r_c = r_c(z)$. The slope is not large, though $dr_c/dz = \tan\left(\frac{1}{2}\theta\right) \approx 0.27$. Considering the electric field force and the gas drag as leading components in the balance then along the cone surface must be [42]

$$F_r|_{r=r_c(z)} \equiv [Z|e|E_r(r,z) - m\gamma_{\mathrm{Eps}}V_r(r,z)]_{r=r_c(z)} = 0. \qquad (4)$$

Since the cluster is transversally narrow, i.e., the transverse electric field is comparatively strong, only the near-axis region $r \ll R(z)$ is of interest. In this case, Eqs. (1), (2), and (4) then yield $\frac{Z|e|E_r}{mg} \approx \frac{\gamma_{\mathrm{Eps}}V_{0z}(z)}{g}\frac{R'(z)}{R(z)}r$. This radial field component is enough to counteract to the transverse component of the gas drag along the cone surface. An approximately parabolic profile of the transverse potential distribution is noticeable. This is a quite expected result [30,31].

C. Interior cluster design

A favorable configuration of external forces, though a necessary condition of the global stable confinement, could not explain the structure and the structural stability of the strings comprising the cluster. A mutual particle-particle attraction, tying the cluster particles into internally stable strings, has to be present.

The strings that the cluster consists of are mostly aligned along the gas flow lines (see Fig. 3), where, to some extent, they are functioning as a windsock or as dangling threads in the wind [43]. This is a quite straightforward indication that the particles, forming a string, must be coupled internally, e.g., by the wake-field forces [1].

The magnitude of the forces, binding the particles, can be estimated as follows. The local "drift" is clearly identifiable (Fig. 4) of the order of $V_D \simeq 2.5$ mm/s in the apex of the cluster. It is reasonable to assume that this drift is due to a deformation-mediated in-string particle rearrangement in response to gas drag. Accordingly, the "spring constant" k of a deformed string can be estimated as (clarified in Ref. [17])

$$k \sim m\gamma_{\mathrm{Eps}}\frac{V_D}{\Delta}. \qquad (5)$$

For our set of parameters it yields $k \sim 600$–700 eV/mm^2, which is close to that obtained in Ref. [17]. Suggestively, the driving mechanism of this kind of activity is similar to that proposed in Ref. [17].

To conclude, we have reported a direct observation of cone-shaped clusters of microparticle strings stably confined in a dc discharge with a nozzle-controlled gas flow. Varying the cluster position by adjusting the gas flux, the strings can be used as a diagnostic tool to determine the electric field inside the nozzle.

ACKNOWLEDGMENTS

The research leading to these results has received funding from the European Research Council under the European Union's Seventh Framework Programme (FP7/2007-2013)/ERC Grant Agreement No. 267499, and by DLR (BMBF) under Grants No. 50WP0204, No. 50WM0504, No. 50WM0804, and No. 50WM1150. The authors would like to thank Dr. P. Huber and Ch. Rau for their help.

[1] G. E. Morfill and A. V. Ivlev, Rev. Mod. Phys. **81**, 1353 (2009).
[2] V. E. Fortov, A. V. Ivlev, S. A. Khrapak, A. G. Khrapak, and G. E. Morfill, Phys. Rep. **421**, 1 (2005).
[3] S. K. Zhdanov, M. H. Thoma, and G. E. Morfill, New J. Phys. **13**, 013039 (2011).
[4] M. Lampe, G. Joyce, G. Ganguli, and V. Gavrishchaka, Phys. Plasmas **7**, 3851 (2000).
[5] A. P. Nefedov, O. F. Petrov, V. I. Molotkov, and V. E. Fortov, JETP Lett. **72**, 218 (2000).
[6] A. V. Ivlev, G. E. Morfill, H. M. Thomas, C. Räth, G. Joyce, P. Huber, R. Kompaneets, V. E. Fortov, A. M. Lipaev, V. I. Molotkov, T. Reiter, M. Turin, and P. Vinogradov, Phys. Rev. Lett. **100**, 095003 (2008).
[7] K. R. Sütterlin, A. Wysocki, A. V. Ivlev, C. Räth, H. M. Thomas, M. Rubin-Zuzic, W. J. Goedheer, V. E. Fortov, A. M. Lipaev, V. I. Molotkov, O. F. Petrov, G. E. Morfill, and H. Löwen, Phys. Rev. Lett. **102**, 085003 (2009).
[8] M. Kroll, J. Schablinski, D. Block, and A. Piel, Phys. Plasmas **17**, 013702 (2010).
[9] C.-R. Du, V. Nosenko, S. Zhdanov, H. M. Thomas, and G. E. Morfill, Europhys. Lett. **99**, 55001 (2012).
[10] L.-W. Teng, P.-S. Tu, and L. I, Phys. Rev. Lett. **90**, 245004 (2003).
[11] O. Arp, D. Block, A. Piel, and A. Melzer, Phys. Rev. Lett. **93**, 165004 (2004).
[12] M. A. Fink, M. Kretschmer, V. Fortov, H. Höfner, U. Konopka, G. E. Morfill, O. Petrov, S. Ratynskaia, A. Usachev, and A. Zobnin, in *New Vistas in Dusty Plasmas*, edited by L. Boufendi, M. Mikikian, and P. K. Shukla, AIP Conf. Proc. Vol. 799 (AIP, Melville, NY, 2005), p. 295.
[13] A. Melzer, Plasma Sources Sci. Technol. **10**, 303 (2001).
[14] A. Melzer, B. Buttenschön, T. Miksch, M. Passvogel, D. Block, O. Arp, and A. Piel, Plasma Phys. Controlled Fusion **52**, 124028 (2010).
[15] A. Wysocki, C. Räth, A. V. Ivlev, K. R. Sütterlin, H. M. Thomas, S. Khrapak, S. Zhdanov, V. E. Fortov, A. M. Lipaev, V. I. Molotkov, O. F. Petrov, H. Löwen, and G. E. Morfill, Phys. Rev. Lett. **105**, 045001 (2010).

[16] P. Ludwig, H. Kählert, and M. Bonitz, Plasma Phys. Controlled Fusion **54**, 045011 (2012).

[17] L. Wörner, C. Räth, V. Nosenko, S. K. Zhdanov, H. M. Thomas, G. E. Morfill, J. Schablinski, and D. Block, Europhys. Lett. **100**, 35001 (2012).

[18] S. Marsh and W. H. Nottage, Proc. Phys. Soc. London **23**, 264 (1910).

[19] E. Rousseau, D. Ponarin, L. Hristakos, O. Avenel, E. Varoquaux, and Y. Mukharsky, Phys. Rev. B **79**, 045406 (2009).

[20] V. E. Fortov, V. I. Molotkov, and A. P. Nefedov, in *Structures in Low Temperature Dusty Plasmas in: Progress in the Physics of Clusters*, edited by G. N. Chuev, V. D. Lakhno, and A. P. Nefedov (World Scientific, Singapore, 1999), p. 6.

[21] B. A. Trubnikov, Plasma Phys. Rep. **28**, 312 (2002).

[22] A. V. Silhanek, M. V. Milosevic, R. B. G. Kramer, G. R. Berdiyorov, J. Van de Vondel, R. F. Luccas, T. Puig, F. M. Peeters, and V. V. Moshchalkov, Phys. Rev. Lett. **104**, 017001 (2010).

[23] A. Couairon and A. Mysyrowicz, Phys. Rep. **441**, 47 (2007).

[24] C. J. Olson Reichhardt, C. Reichhardt, and A. R. Bishop, Phys. Rev. Lett. **92**, 016801 (2004).

[25] P. Holme and J. Saramäki, Phys. Rep. **519**, 97 (2012).

[26] J. P. Dietrich, N. Werner, D. Clowe, A. Finoguenov, T. Kitching, L. Miller, and A. Simionescu, Nature (London) **487**, 202 (2012).

[27] S. Mitic, R. Sütterlin, A. V. Ivlev, H. Höfner, M. H. Thoma, S. Zhdanov, and G. E. Morfill, Phys. Rev. Lett. **101**, 235001 (2008).

[28] M. Schwabe, L.-J. Hou, S. Zhdanov, A. V. Ivlev, H. M. Thomas, and G. E. Morfill, New J. Phys. **13**, 083034 (2011).

[29] H. Kählert, J. Carstensen, M. Bonitz, H. Löwen, F. Greiner, and A. Piel, Phys. Rev. Lett. **109**, 155003 (2012).

[30] A. Usachev, A. Zobnin, O. Petrov, V. Fortov, M. Thoma, M. Kretschmer, S. Ratynskaia, R. Quinn, H. Höfner, and G. E. Morfill, Czech. J. Phys. **54**, C639 (2004).

[31] V. Fortov, G. Morfill, O. Petrov, M. Thoma, A. Usachev, H. Höfner, A. Zobnin, M. Kretschmer, S. Ratynskaia, M. A. Fink, K. Tarantik, Yu. Gerasimov, and V. Esenkov, Comments Plasma Phys. Controlled Fusion **47**, B537 (2005).

[32] P. S. Epstein, Phys. Rev. **23**, 710 (1924).

[33] G. E. Morfill, U. Konopka, M. Kretschmer, M. Rubin-Zuzic, H. M. Thomas, S. K. Zhdanov, and V. Tsytovich, New J. Phys. **8**, 7 (2006).

[34] S. A. Khrapak, S. V. Ratynskaia, A. V. Zobnin, A. D. Usachev, V. V. Yaroshenko, M. H. Thoma, M. Kretschmer, H. Höfner, G. E. Morfill, O. F. Petrov, and V. E. Fortov, Phys. Rev. E **72**, 016406 (2005).

[35] M. E. Bannister, D. W. Mueller, L. J. Wang, M. S. Pindzola, D. C. Griffin, and D. C. Gregory, Phys. Rev. A **38**, 38 (1988).

[36] L. Sirghi, K. Ohe, and G. Popa, J. Phys. D **30**, 2431 (1997).

[37] A. V. Ivlev, S. K. Zhdanov, S. A. Khrapak, and G. E. Morfill, Phys. Rev. E **71**, 016405 (2005).

[38] J. A. Hornbeck and G. H. Wannier, Phys. Rev. **82**, 458 (1951).

[39] H. Lamb, *Hydrodynamics*, 6th ed. (Dover, New York, 1945); L. D. Landau and E. M. Lifshitz, *Fluid Mechanics*, 2nd ed. (Elsevier, Amsterdam, 1987).

[40] The electric field force considered here is introduced as an effective value that is *including* the ion drag force [37]; the latter does not exceed 20% of the total force in our conditions, and is smaller than the error bars (see Fig. 3).

[41] M. Schwabe, M. Rubin-Zuzic, S. Zhdanov, H. M. Thomas, and G. E. Morfill, Phys. Rev. Lett. **99**, 095002 (2007).

[42] The pressure gradient forces are small in our conditions, albeit they have been found important, e.g., in robotics enabling noncontact stable manipulation of the macroobjects [A. Becker, R. Sandheinrich, and T. Bretl, in *IEEE-RSJ International Conference on Intelligent Robots and Systems* (IEEE, New York, 2009), p. 718].

[43] See Supplemental Material at http://link.aps.org/supplemental/10.1103/PhysRevE.86.065401 for a movie of the particle cluster.